



Article

Hybrid Nanofluid Flow Past a Shrinking Cylinder with Prescribed Surface Heat Flux

Najiyah Safwa Khashi'ie ¹, Iskandar Waini ^{1,*}, Nurul Amira Zainal ¹, Khairum Hamzah ¹
and Abdul Rahman Mohd Kasim ²

¹ Fakulti Teknologi Kejuruteraan Mekanikal dan Pembuatan, Universiti Teknikal Malaysia Melaka, Hang Tuah Jaya, Durian Tunggal 76100, Melaka, Malaysia; najiyah@utem.edu.my (N.S.K.); nurulamira@utem.edu.my (N.A.Z.); khairum@utem.edu.my (K.H.)

² Centre for Mathematical Sciences, College of Computing & Applied Sciences, Universiti Malaysia Pahang, Lebuhraya Tun Razak, Gambang 26300, Pahang, Malaysia; rahmanmohd@ump.edu.my

* Correspondence: iskandarwaini@utem.edu.my

Received: 4 August 2020; Accepted: 25 August 2020; Published: 10 September 2020



Abstract: This numerical study was devoted to examining the occurrence of non-unique solutions in boundary layer flow due to deformable surfaces (cylinder and flat plate) with the imposition of prescribed surface heat flux. The hybrid $\text{Al}_2\text{O}_3\text{-Cu}$ /water nanofluid was formulated using the single phase model with respective correlations of hybrid nanofluids. The governing model was simplified by adopting a similarity transformation. The transformed differential equations were then numerically computed using the efficient bvp4c solver with the ranges of the control parameters $0.5\% \leq \phi_1, \phi_2 \leq 1.5\%$ (Al_2O_3 and Cu volumetric concentration), $0 \leq K \leq 0.2$ (curvature parameter), $2.6 < S \leq 3.2$ (suction parameter) and $-2.5 < \lambda \leq 0.5$ (stretching/shrinking parameter). Dual steady solutions are presentable for both a cylinder ($K > 0$) and a flat plate ($K = 0$) with the inclusion of only the suction (transpiration) parameter. The real and stable solutions were mathematically validated through the stability analysis. The $\text{Al}_2\text{O}_3\text{-Cu}$ /water nanofluid with $\phi_1 = 0.5\%$ (alumina) and $\phi_2 = 1.5\%$ (copper) has the highest skin friction coefficient and heat transfer rate, followed by the hybrid nanofluids with volumetric concentrations ($\phi_1 = 1\%, \phi_2 = 1\%$) and ($\phi_1 = 1.5\%, \phi_2 = 0.5\%$), respectively. Surprisingly, the flat plate surface abates the separation of boundary layer while it enhances the heat transfer process.

Keywords: hybrid nanofluid; permeable cylinder; stretching/shrinking; heat flux; dual solutions

1. Introduction

Over recent decades, the investigation in the field of fluid flow has gained interest due to the wide range of industrial applications. The explorations so far have covered Newtonian and non-Newtonian fluids with multiple effects and single or multi-phases [1–5]. The applications of the study of fluid flow can be found in mechanical and chemical engineering, biological systems and astrophysics. The inquisitiveness in this field grew significantly in the past few years after Choi [6] embedded the nanoparticle in the investigation of fluid flow to develop an advanced heat transfer fluid with substantially higher conductivities. The analysis revealed that the fluid with nanoparticles enhanced the thermophysical properties as compared to the classical working fluid. Since then, many researchers gained interest and contributed to this field by considering experimental and numerical studies. Wang and Su [7] conducted an experimental study on the boiling heat transfer of a nanofluid in a vertical tube with diverse pressure conditions. The continuation of the study has been reported in Wang et al. [8]. The experimental works on nanofluids also have been documented by Ahmadi and Willing [9], Masuda et al. [10], Das et al. [11] and Pak and Cho [12]. Meanwhile, study via

a mathematical approach with various effects and surfaces was reported in work done by Kuznetsov and Nield [13], Mahat et al. [14], Zokri et al. [15] and Waini et al. [16].

As nanofluids are extensively used as coolants; lubricants; and also in practical applications, including refrigeration, air-conditioning, microelectronics and processors of mobile computers, the advancements in this topic are being further investigated by considering fluids containing more than one type of nanoparticle called hybrid nanofluids. This new invention has new thermal characteristics as compared to conventional nanofluids. The application of $\text{Al}_2\text{O}_3\text{-Cu/water}$ in the boundary layer flow was further analyzed by Waini et al. [17,18] for thin needle and sensor surfaces, respectively; Khashi'ie et al. [19,20] for Riga plate and cylinder surfaces, respectively; and Zainal et al. [21–23] specifically for the flat plate cases. They also performed a stability analysis to justify the stability of the dual solutions. Moreover, the collection of documents on hybrid nanofluids can be found in works done by Yen et al. [24], Labib et al. [25], Nasrin and Alim [26], Takabi and Shokouhmand [27], Devi and Devi [28,29], Yousefi et al. [30], Hayat et al. [31], Ghadikolaei et al. [32], Tayebi and Chamkha [33] and Ashorynejad and Shahriari [34].

According to the current studies on the fluid mechanics of fluid flow, the flow characteristics depend on what type of geometry the fluid is moving over. A group of researchers focused on the fluid flow problem over different types of stretching/shrinking surfaces. For instance, Kasim et al. [35] investigated the interaction on a fluid and solid moving over a stretching sheet, and Lund et al. [36] considered the study of fluid flow past an inclined stretching/shrinking surface. Waini et al. [37] and Anuar et al. [38] deliberated on the problem of fluid flow under an exponentially shrinking sheet. The fluid flow passing over a shrinking cylinder was first discussed by Wang [39]. The exponential transformation was used to facilitate numerical integration in order to compute the solution. His work was further investigated by Mukhopadhyay [40], Vajravelu et al. [41], Butt and Ali [42], Abbas et al. [43], Malik et al. [44] and Shafik et al. [45]. Besides, the problem of the flow past a cylinder has important applications in the study of geological formations that includes the exploration and thermal recovery of oil, geothermal reservoirs and underground nuclear waste storage sites. The outcomes from this study will be beneficial to the engineers in the prediction of flow, heat transfer and solute or contaminant dispersion about intrusive bodies such as salt domes, magnetic intrusions, piping and casting systems (see Ganesan and Loganathan [46]). Recent works on flow past a stretching cylinder with various physical phenomena can be found in Ferdows et al. [47] (gyrotactic microorganism), Ullah et al. [48] (chemical reaction and heat generation/absorption) and Suleman et al. [49] (homogeneous-heterogeneous reactions).

The choices of the thermal boundary conditions for the fluid flow problem are very crucial, since a difference in conditions leads one to describe a different situation for the problem. They are four types of boundary conditions which are generally used. They are constant wall temperature (CWT), constant/prescribe heat flux (PHF), Newtonian heating (NH) and convective boundary condition (CBC). According to Muthamilselvan and Prakash [50], the constant thermal boundary conditions that are imposed on the surface are not adequate in some cases, for example, in a microelectromechanical (MEM) condensation application where a fixed heat dissipation due to condensation on the lower surface of the plate is removed by the gas flowing over the top surface. Therefore, a lot of research work was replaced with a different heating process. The condition of CWT is generally used to describe bodies with very high heat conductivity while PHF is used to present the problem with the supplied thermal energy from the surface. The NH and CBC correspond to the existence of convection heating (or cooling) at the surface and are obtained from the surface energy balance. They are many reported articles that considered those thermal boundary conditions. The present problem considered the case of PHF, since it seems more realistic. The existing studies involving the particular thermal boundary condition can be found in [51–55].

Motivated by the above literature, the present paper aims to extend the existing investigation of hybrid nanofluids by considering the flow past a shrinking cylinder through adopting the model of nanofluids proposed by Tiwari and Das [56]. The hybrid nanofluid deliberated with two elements,

which were Al_2O_3 and Cu in pure water. The governing equations with thermal condition heat flux were first transformed into a system of ordinary differential equations by using an appropriate similarity transformation. The system of equations was then solved numerically using the boundary value problem solver (bvp4c) which is embedded in Matlab software. The validation of the present works was done by direct comparison with the current output in the literature for special cases (limiting cases). The effects of pertinent parameters on the flow and heat transfer characteristics are presented in tabular and graphical form. To the best of the authors' knowledge, minimal studies have been reported in the literature regarding the investigation of flow over a shrinking cylinder in hybrid nanofluids embedded in the heat flux thermal condition.

2. Mathematical Formulation

A steady, incompressible and laminar boundary layer flow of hybrid nanofluid (Cu- Al_2O_3 /water) towards a horizontal cylinder is studied here. The circular cylinder with radius a is deformed (stretch/shrink) with velocity $u_w(x) = u_0x/L$ where constant u_0 is a characteristic velocity and L is the characteristic length of the cylinder. Figure 1 illustrates the physical model and coordinate system (x, r) of this problem. The deformable cylinder is subjected to the prescribed heat flux $q_w(x) = T_0x/L$ where T_0 is a characteristic temperature.

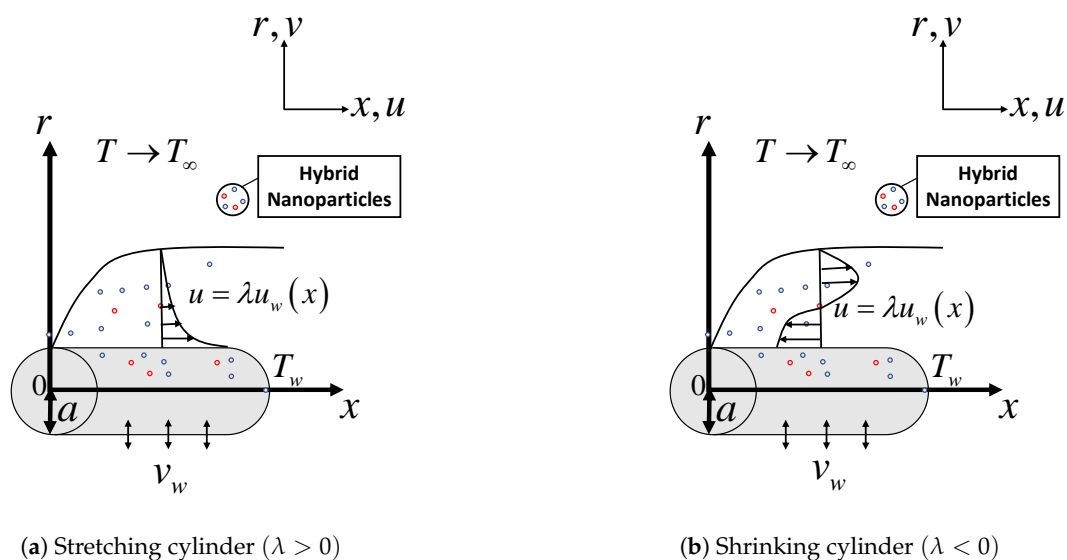


Figure 1. The coordinate system and physical models of (a) the stretching cylinder and (b) the shrinking cylinder.

The governing model in the PDEs (partial differential equations) is given as (see Khashi'ie et al. [20], Qasim et al. [57])

$$\frac{\partial(ru)}{\partial x} + \frac{\partial(rv)}{\partial r} = 0, \quad (1)$$

$$u \frac{\partial u}{\partial x} + v \frac{\partial u}{\partial r} = \frac{\mu_{hnf}}{\rho_{hnf}} \left(\frac{\partial^2 u}{\partial r^2} + \frac{1}{r} \frac{\partial u}{\partial r} \right), \quad (2)$$

$$u \frac{\partial T}{\partial x} + v \frac{\partial T}{\partial r} = \frac{k_{hnf}}{(\rho C_p)_{hnf}} \left(\frac{\partial^2 T}{\partial r^2} + \frac{1}{r} \frac{\partial T}{\partial r} \right), \quad (3)$$

while the boundary conditions are

$$\begin{aligned} v = v_w(r), \quad u = \lambda u_w(x), \quad k_{hnf} \frac{\partial T}{\partial r} = -q_w(x), \quad \text{at } r = a \\ u \rightarrow 0, \quad T \rightarrow T_\infty, \quad \text{as } r \rightarrow \infty \end{aligned} \quad (4)$$

where $v_w(r)$ represents the mass flux velocity through the permeable surface such that $v_w(r) > 0$ for mass injection and $v_w(r) < 0$ for mass suction. For the case of an impermeable surface, $v_w(r) = 0$. Besides, u and v denote the velocities along x - and r -axes, correspondingly and T is the temperature of the hybrid nanofluid. In this work, the constant far-field temperature T_∞ is considered while the cylinder wall is subjected to the variable heat flux $q_w(x)$. In addition, the constant stretching/shrinking parameter λ signifies the shrinking cylinder when $\lambda < 0$ and stretching cylinder when $\lambda > 0$. The static cylinder is symbolized by $\lambda = 0$. The correlations of the nanofluids (regular and hybrid) are presented in Table 1 where s_1 and s_2 denote the alumina and copper nanoparticles, respectively; ϕ_1 and ϕ_2 are the volumetric concentrations of the alumina and copper nanoparticles, accordingly. Besides, the subscript bf denotes the base fluid (pure water); nf and hnf are single and hybrid nanofluids, respectively. In Table 1, $\phi_{hnf} = \phi_1 + \phi_2$ where $\phi_{hnf} \approx 0$ corresponds to water—base fluid. The thermophysical properties of the water and both nanoparticles are presented in Table 2.

Table 1. The correlations of single (nf) and hybrid nanofluids (hnf) (see Tiwari and Das [56], Takabi and Salehi [58]).

Properties	Nanofluids
Density (ρ)	$\rho_{nf} = (1 - \phi) \rho_{bf} + \phi \rho_s$
	$\rho_{hnf} = (1 - \phi_{hnf}) \rho_{bf} + \phi_1 \rho_{s1} + \phi_2 \rho_{s2}$
Heat Capacity (ρC_p)	$(\rho C_p)_{nf} = (1 - \phi)(\rho C_p)_{bf} + \phi(\rho C_p)_s$
	$(\rho C_p)_{hnf} = (1 - \phi_{hnf})(\rho C_p)_{bf} + \phi_1(\rho C_p)_{s1} + \phi_2(\rho C_p)_{s2}$
Dynamic Viscosity (μ)	$\frac{\mu_{nf}}{\mu_{bf}} = \frac{1}{(1 - \phi)^{2.5}}$
	$\frac{\mu_{hnf}}{\mu_{bf}} = \frac{1}{(1 - \phi_{hnf})^{2.5}}$
Thermal Conductivity (k)	$\frac{k_{nf}}{k_{bf}} = \left[\frac{k_s + 2k_{bf} - 2\phi(k_{bf} - k_s)}{k_s + 2k_{bf} + \phi(k_{bf} - k_s)} \right]$
	$\frac{k_{hnf}}{k_{bf}} = \left[\frac{\frac{\phi_1 k_1 + \phi_2 k_2}{\phi_{hnf}} + 2k_{bf} + 2(\phi_1 k_1 + \phi_2 k_2) - 2\phi_{hnf} k_{bf}}{\frac{\phi_1 k_1 + \phi_2 k_2}{\phi_{hnf}} + 2k_{bf} - (\phi_1 k_1 + \phi_2 k_2) + \phi_{hnf} k_{bf}} \right]$

Table 2. Thermo-physical properties of the nanoparticles and water (see Oztop and Abu-Nada [59]).

Thermophysical Properties	Nanoparticles		
	Base Fluid Pure Water	Alumina	Copper
C_p (J/kgK)	4179	765	385
ρ (kg/m ³)	997.1	3970	8933
k (W/mK)	0.6130	40	400

The following similarity variables are introduced as (Qasim et al. [57], Giri et al. [60])

$$u = \frac{u_0 x}{L} f'(\eta), \quad v = -\frac{a}{r} \sqrt{\frac{u_0 v_f}{L}} f(\eta), \quad T = T_\infty + \frac{q_w}{k_f} \sqrt{\frac{v_f L}{u_0}} \theta(\eta), \quad \eta = \sqrt{\frac{u_0}{v_f L}} \frac{r^2 - a^2}{2a}, \quad (5)$$

so that

$$v_w(r) = -\frac{a}{r} \sqrt{\frac{u_0 v_f}{L}} S, \quad (6)$$

where v_f is the kinematic viscosity of the water, S is the dimensionless mass flux parameter and categorized as $S > 0$ and $S < 0$ for suction and injection, respectively. The continuity equation

in Equation (1) is obeyed by adopting the transformation in Equation (5). Hence, considering this transformation, Equations (2)–(4) are transformed and simplified to

$$\frac{\mu_{hmf}/\mu_f}{\rho_{hmf}/\rho_f} [(1 + 2K\eta)f'' + 2Kf''] + ff'' - f'^2 = 0, \quad (7)$$

$$\frac{1}{\text{Pr}} \frac{k_{hmf}/k_f}{(\rho C_p)_{hmf}/(\rho C_p)_f} [(1 + 2K\eta)\theta'' + 2K\theta'] + f\theta' - f'\theta = 0, \quad (8)$$

$$f'(0) = \lambda, \quad f(0) = S, \quad \theta'(0) = -\frac{k_f}{k_{hmf}}, \quad (9)$$

$$f'(\infty) \rightarrow 0, \quad \theta(\infty) \rightarrow 0,$$

where $K = \sqrt{v_f L / u_0 a^2}$ is the curvature parameter and $\text{Pr} = (\mu C_p)_f / k_f$ is the Prandtl number. The local skin friction coefficient C_f and the local Nusselt number Nu_x (heat transfer rate) are defined as

$$C_f = \frac{\mu_{hmf}}{\rho_f u_w^2} \left(\frac{\partial u}{\partial r} \right)_{r=a}, \quad Nu_x = -\frac{x k_{hmf}}{k_f (T_w - T_\infty)} \left(\frac{\partial T}{\partial r} \right)_{r=a}. \quad (10)$$

By substituting Equation (5) into Equation (10), we obtain

$$Re_x^{1/2} C_f = \frac{\mu_{hmf}}{\mu_f} f''(0), \quad Re_x^{-1/2} Nu_x = \frac{1}{\theta(0)} \quad (11)$$

where $Re_x = u_w(x)x/v_f$ is the local Reynolds number.

3. Stability Analysis

Consider an unsteady problem of Equations (2) and (3) to test the stability of the particular similarity solutions such that

$$\frac{\partial u}{\partial t} + u \frac{\partial u}{\partial x} + v \frac{\partial u}{\partial r} = \frac{\mu_{hmf}}{\rho_{hmf}} \left(\frac{\partial^2 u}{\partial r^2} + \frac{1}{r} \frac{\partial u}{\partial r} \right), \quad (12)$$

$$\frac{\partial T}{\partial t} + u \frac{\partial T}{\partial x} + v \frac{\partial T}{\partial r} = \frac{k_{hmf}}{(\rho C_p)_{hmf}} \left(\frac{\partial^2 T}{\partial r^2} + \frac{1}{r} \frac{\partial T}{\partial r} \right). \quad (13)$$

The disturbance in a solution may grow or decay with time; hence, it is worth using an unsteady model. The relevant similarity transformation which is applicable to reducing Equations (12) and (13) is

$$u = \frac{u_0 x}{L} \frac{\partial f(\eta, \tau)}{\partial \eta}, \quad v = -\frac{a}{r} \sqrt{\frac{u_0 v_f}{L}} f(\eta, \tau), \quad T = T_\infty + \frac{q_w}{k_f} \sqrt{\frac{v_f L}{u_0}} \theta(\eta, \tau), \quad \eta = \sqrt{\frac{u_0}{v_f L}} \frac{r^2 - a^2}{2a}, \quad (14)$$

where $\tau = u_0 t / L$ is a time variable. Thus, the reduced differential equations including the boundary conditions are

$$\frac{\mu_{hmf}/\mu_f}{\rho_{hmf}/\rho_f} \left[(1 + 2K\eta) \frac{\partial^3 f}{\partial \eta^3} + 2K \frac{\partial^2 f}{\partial \eta^2} \right] + f \frac{\partial^2 f}{\partial \eta^2} - \left(\frac{\partial f}{\partial \eta} \right)^2 - \frac{\partial^2 f}{\partial \eta \partial \tau} = 0, \quad (15)$$

$$\frac{1}{\text{Pr}} \frac{k_{hmf}/k_f}{(\rho C_p)_{hmf}/(\rho C_p)_f} \left[(1 + 2K\eta) \frac{\partial^2 \theta}{\partial \eta^2} + 2K \frac{\partial \theta}{\partial \eta} \right] + f \frac{\partial \theta}{\partial \eta} - \theta \frac{\partial f}{\partial \eta} - \frac{\partial \theta}{\partial \tau} = 0, \quad (16)$$

$$f(0, \tau) = S, \quad \frac{\partial f(0, \tau)}{\partial \eta} = \lambda, \quad \frac{\partial \theta(0, \tau)}{\partial \eta} = -\frac{k_f}{k_{hf}}, \quad \frac{\partial f(\infty, \tau)}{\partial \eta} \rightarrow 0, \quad \theta(\infty, \tau) \rightarrow 0. \quad (17)$$

Further, to examine the solution's stability, the following perturbation equations in (18) can be substituted into Equations (15)–(17) to generate a list of unknown eigenvalues β where $\beta_1 < \beta_2 < \dots < \beta_n$. The positive or negative sign from the smallest eigenvalue β_1 is important in determining a solution's stability. The perturbation equations are (Merkin [61], Weidman et al. [62])

$$f(\eta, \tau) = f_0(\eta) + e^{-\beta\tau}F(\eta), \quad \theta(\eta, \tau) = \theta_0(\eta) + e^{-\beta\tau}G(\eta), \quad (18)$$

where $f_0(\eta) = f(\eta)$, $\theta_0(\eta) = \theta(\eta)$; and $F(\eta)$ and $G(\eta)$ are small relatives to $f_0(\eta)$ and $\theta_0(\eta)$, respectively. The linearized eigenvalue problem is represented by

$$\frac{\mu_{hf}/\mu_f}{\rho_{hf}/\rho_f} [(1 + 2K\eta)F''' + 2KF''] + F''f_0 - (2f_0' - \beta)F' + f_0''F = 0, \quad (19)$$

$$\frac{1}{Pr} \frac{k_{hf}/k_f}{(\rho C_p)_{hf}/(\rho C_p)_f} [(1 + 2K\eta)G'' + 2KG'] + G'f_0 + (\beta - f_0')G - \theta_0 F' + F\theta_0' = 0, \quad (20)$$

and the homogeneous boundary condition is

$$\begin{aligned} F(0) = 0, \quad G'(0) = 0, \quad F'(0) = 0, \\ F'(\infty) \rightarrow 0, \quad G(\infty) \rightarrow 0. \end{aligned} \quad (21)$$

As recommended by Harris et al. [63], the trivial eigenvalue solution can be prevented by replacing and relaxing $F'(\infty) \rightarrow 0$ in Equation (21) with $F''(0) = 1$. $\beta_1 > 0$ implies that the solution is stable and realistic while $\beta_1 < 0$ concludes that the solution is unreal or unstable.

4. Results and Discussion

The essential factor for the computation of flow behaviors and the heat transfer performance of a nanofluid is the preparation of appropriate mono/hybrid nanofluids. The selection of alumina-copper/water ($\text{Al}_2\text{O}_3\text{-Cu/water}$) hybrid nanofluid in this study was motivated by Suresh et al. [64] who set up an experiment to examine the thermophysical properties of $\text{Al}_2\text{O}_3\text{-Cu/water}$ hybrid nanofluids. Their investigational work proved that the stability of a hybrid nanofluid relies on the nanoparticles' volume concentration, and the stability of a nanofluid with a higher concentration is poor. Additionally, the experimental results indicate that the prepared hybrid nanofluid substantially improved in efficiency of thermal conductivity and stability. Thus, the impacts of the aggregation and sedimentation of mono/hybrid nanoparticles can be ignored in this numerical work. It is worth mentioning that the Prandtl number was fixed at 6.2 (representing water) throughout the analysis of this study (Oztop and Abu Nada [59]). Obeying the remarkable work of Suresh et al. [64], the nanoparticles' volume concentration of this study was set within the range of $0.005 \leq \phi_1, \phi_2 \leq 0.015$ to ensure the stability of the hybrid nanofluid. Meanwhile, the other parameters were used between these ranges (excluding the validation part): $0 \leq K \leq 0.2$ (curvature parameter), $2.6 < S \leq 3.2$ (suction parameter) and $-2.5 < \lambda \leq 0.5$ (stretching/shrinking parameter). Further, the bvp4c in Matlab was fully utilized to solve the ordinary and reduced differential equation systems of Equations (7) and (8) together with the boundary equations (see Equation (9)). This recognized solver has been utilized extensively by many other investigators to address the boundary value issue. With the aim of achieving the required precision of the solutions, an initial approximation shall be offered at an initial mesh point and for a certain step size. The appropriate initial approximation and the thickness of the boundary layer η_∞ must be selected in accordance with the values of the parameter listed.

In pursuance of the numerical outcomes, verification and accuracy of the utilized method, i.e., bvp4c, the comparison values of $\theta(0)$ when $S = 0$, $\lambda = 1$ and $\phi_1, \phi_2 \approx 0$ (viscous fluid) with a different value of the curvature parameter K were assessed and are presented in Table 3. It is important to note here when $K = 0$ the cylindrical surface is reduced to a flat plate, while the increment value of K , i.e., $K = 1$ denotes as a cylinder with 100% curvature. Table 4 provides the comparison values of $Re_x^{1/2}C_{fx}$ when $K = 0$ (flat plate), $S = 2.5$, $\lambda = -1$, $Pr = 6.2$, $\phi_1 = 0.1$ and various ϕ_2 , and it is evident that the obtained results are in outstanding agreement with the formerly published results of Qasim et al. [57], Khashi'ie et al. [65] and Bachok et al. [64]. The results of several parameters on the coefficient of skin friction and the local Nusselt number together with the velocity and temperature profiles are provided by Figures 2–13 in graphical form. The impacts of the curvature parameter and various nanoparticles volumetric concentrations towards the suction/injection parameter and the stretching/shrinking parameter are discussed in detail. As a matter of fact, this current work confirms the existence of dual solutions, i.e., the first and second solutions, and a unique solution for a certain range of controlling parameters.

Table 3. Comparison values of $\theta(0)$ when $S = 0$, $\lambda = 1$ and $\phi_1, \phi_2 \approx 0$ (viscous fluid).

K	Pr	Present	Qasim et al. [57]	Bachok et al. [66]
0.0	0.72	1.23666	1.23664	1.2367
	1.0	1.00000	1.00000	1.0000
	6.7	0.33330	0.33330	0.3333
	10	0.26877	0.26876	0.2688
1.0	0.72	0.87058	0.87018	0.8701
	1.0	0.74395	0.74406	0.7439
	6.7	0.29653	0.29661	0.2966
	10.0	0.24412	0.24217	0.2442

Table 4. Comparison values of $Re_x^{1/2}C_{fx}$ when $K = 0$, $S = 2.5$, $\lambda = -1$, $Pr = 6.2$, $\phi_1 = 0.1$ and various ϕ_2 .

ϕ_2	Present		Khashi'ie et al. [65]	
	First Solution	Second Solution	First Solution	Second Solution
0	2.594177	0.645222	2.594178	0.645222
0.01	2.781516	0.655350	2.781516	0.655350
0.02	2.967257	0.666893	2.967257	0.666894
0.03	3.151544	0.679725	3.151544	0.679725

Figures 2 and 3 depict the variation of $Re_x^{1/2}C_f$ and $Re_x^{-1/2}Nu_x$ towards S when $\lambda = -1.9$, $\phi_1 = \phi_2 = 0.01$ with different values of the curvature parameter where $K = 0.0, 0.1, 0.2$ in Al_2O_3-Cu/H_2O hybrid nanofluid, respectively. The results of $Re_x^{1/2}C_f$ rise with the intensification of K in the first solution, and decrease in the second solution when the cylinder is in the shrinking state, as demonstrated in Figure 2. Similar outcome patterns for both solutions can also be found in $Re_x^{-1/2}Nu_x$, as evaluated in Figure 3. The deployment of appropriate wall mass suction parameters ($S > 0$) in the present work was able to produce the dual similarity solutions, which is clearly proven in Figures 2 and 3. On the other hand, in the state of the impermeable cylinder where no suction/injection parameter is being considered ($S = 0$) or if the injection parameter ($S < 0$) is added, no equivalent solutions can be achieved, including the unique or dual solutions. Notably, Figure 2 also illustrates that when K upsurges, the additional value of suction parameter S (more magnitude) is required in Al_2O_3-Cu/H_2O hybrid nanofluid. In the present work, however, the authors merely evaluated the value of K within the scope of $0 \leq K \leq 0.2$ in Al_2O_3-Cu /water hybrid nanofluid, and the authors would like to declare that the outcome could be varied if different values of the curvature parameter or distinctive type of hybrid nanofluid are measured. Surprisingly, Figure 3 reveals that the

inclusion of K in the shrinking cylinder eventually declines the heat transfer rate of $\text{Al}_2\text{O}_3\text{-Cu}$ /water hybrid nanofluid. The results oppose the fact that the augmentation in K supposedly improves the heat transfer performance in a nanofluid. This is because the increase in curvature parameter causes diminution of the curvature radius, which consequently lessens the area of the cylinder. The cylinder encounters less resistance from the fluid particles, increases the fluid velocity and ultimately boosts the rate of heat transfer. However, the authors believe that the selection of governing parameter values and the presence of prescribing heat flux at the shrinking surface of the cylinder are the explanations for this behavior. The presence of prescribed heat flux at the boundary condition system imposes some amount of heat flowing, and this consequently may worsen the process of heat transfer. Overall, the $\text{Al}_2\text{O}_3\text{-Cu}$ /water hybrid nanofluid has better heat transfer efficiency in a flat plate ($K = 0$) compared to the cylinder case ($K = 0.1, 0.2$).

Figures 4 and 5 display the diversity of $\text{Re}_x^{1/2}C_f$ and $\text{Re}_x^{-1/2}\text{Nu}_x$ towards λ when $S = 3$, $\phi_1 = \phi_2 = 0.01$ with distinct values of K in $\text{Al}_2\text{O}_3\text{-Cu}$ /water hybrid nanofluid. The dual solutions are observed in the shrinking surface where $\lambda < 0$, whereas no dual solutions can be perceived when the surface is stretching, i.e., $\lambda > 0$. Figure 4 proves that an increment of K decreases $\text{Re}_x^{1/2}C_f$ in the first solution, but upsurges the results in the second solution. Meanwhile, Figure 5 portrays the heat transfer rate of the shrinking surface where $\text{Re}_x^{-1/2}\text{Nu}_x$ is clearly diminished when the values of K rises in $\text{Al}_2\text{O}_3\text{-Cu}/\text{H}_2\text{O}$ hybrid nanofluid. From here, we note that the same pattern is observed in Figures 2 and 3, when K increases. However, these results may vary if different values of the controlling parameter are taken into account. On another note, the effect of the volumetric concentration is also examined in this study. It was observed that the $\text{Re}_x^{1/2}C_f$ and $\text{Re}_x^{-1/2}\text{Nu}_x$, as presented in Figures 6 and 7, respectively, improve with the rise of the Cu nanoparticle concentration in the first solution. In fact, the higher concentration of Cu nanoparticles creates more kinetic energy, and thereby increases the heat transfer of the fluid particles. Nevertheless, Figures 6 and 7 also disclose that the second solution can be obtained only for a small value of negative λ in the opposing or shrinking region.

Figures 8–13 establish the distribution of temperature $\theta(\eta)$ and velocity profiles $f'(\eta)$ with different controlling parameter, for instance, the suction/injection parameter S , the curvature parameter K and the stretching/shrinking parameter λ . All profiles asymptotically fulfilled the boundary condition (9) when $\eta_\infty = 20$ is implemented. Figures 8 and 9 depict the impact of S on $f'(\eta)$ and $\theta(\eta)$, accordingly. The findings show that the increasing value of S is proven to boost the resistance of the flow in $f'(\eta)$ of the first solution; however, an opposite behaviour is observed in the second solution. Meanwhile, Figure 9 exposes a reduction trend of $\theta(\eta)$ in the first and second solutions. The temperature distribution with the inclusion of the suction parameter is discussed to inspect the deterioration in temperature, which hence cools the system. As the temperature of the system reduces, the heat transfer rate is enhanced, and this is proven in Figure 3 above.

Figures 10 and 11 exhibit the variation of K on $f'(\eta)$ and $\theta(\eta)$, appropriately. $f'(\eta)$ is reduced in the first solution but decreases (second solution) when K is added, as displayed in Figure 10. Figure 11 illustrates the rises of $\theta(\eta)$ with increments of K in both solutions, i.e, the first and second solutions. The reduction in the fluid velocity and the increases of temperature profiles are inline with the results obtained in Figure 3, where the addition of K in the shrinking state at last worsens the heat transfer rate of $\text{Al}_2\text{O}_3\text{-Cu}$ /water hybrid nanofluid. Further, the influences of the static cylinder ($\lambda = 0$), the stretching parameter ($\lambda = 0.3, 0.5$) and the shrinking parameter ($\lambda = -0.3, -0.5$) on the velocity and temperature profiles are illustrated in Figures 12 and 13. The findings reveal a unique solution, and no second solution appeared in either profile. That obviously indicates that the changes in behavior from shrinking to stretching state in the cylinder concurrently increase $f'(\eta)$, as clarified in Figure 12. Meanwhile, the temperature profiles $\theta(\eta)$ decrease with the enhancement of the stretching/shrinking parameter λ .

A temporal stability analysis was conducted by solving the linearized eigenvalue problem in (19)–(21) with the inclusion of the new boundary condition $F''(0) = 1$. The results in Figure 14 exhibit that the first solution has $\beta_1 > 0$ (positive smallest eigenvalues). The second solution contributes to

the negative smallest eigenvalue. This shows that the first solution is more realistic than the second solution. Meanwhile, as $\lambda \rightarrow \lambda_c$, $\beta_1 \rightarrow 0$ from both solutions, which is in accordance with Merkin [61] and Weidman et al. [62], the transitions from stable ($\beta_1 > 0$) to unstable ($\beta_1 < 0$) occur at the turning point $\lambda = \lambda_c$.

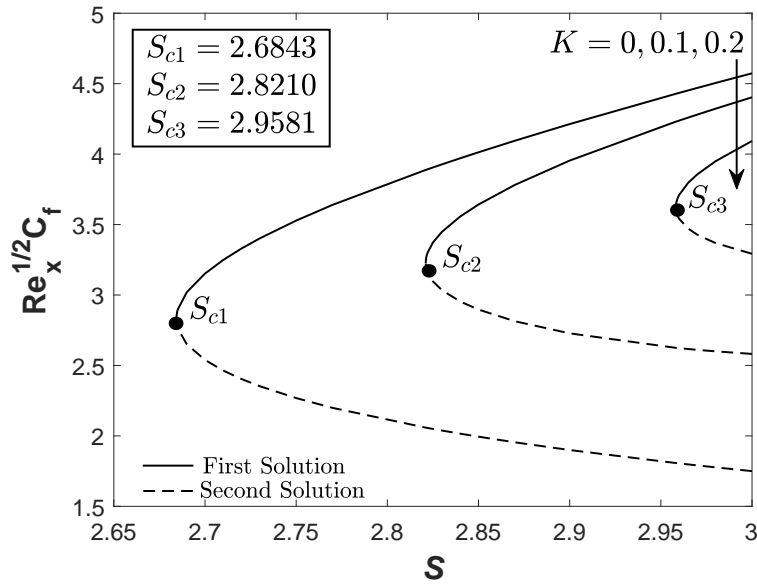


Figure 2. $Re_x^{1/2}C_f$ towards S when $\lambda = -1.9$, $\phi_1 = \phi_2 = 0.01$ and disparate values of the curvature parameter K .

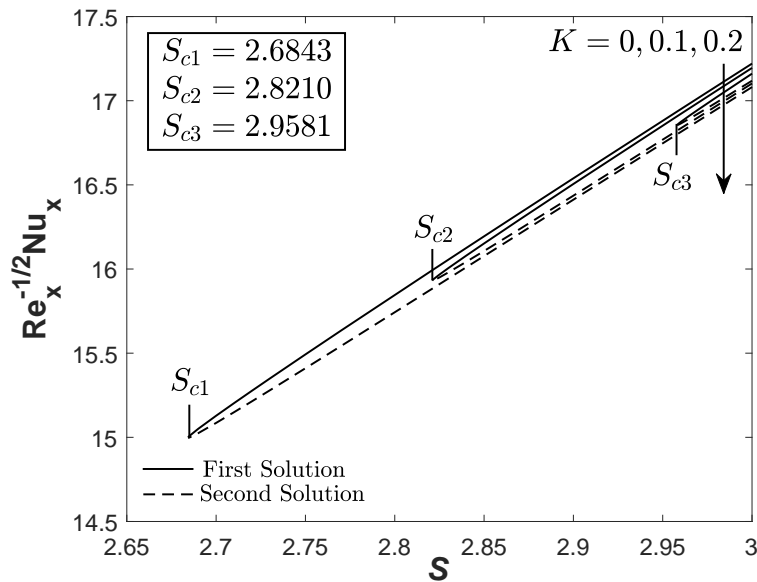


Figure 3. $Re_x^{-1/2}Nu_x$ towards S when $\lambda = -1.9$, $\phi_1 = \phi_2 = 0.01$ and disparate values of the curvature parameter K .

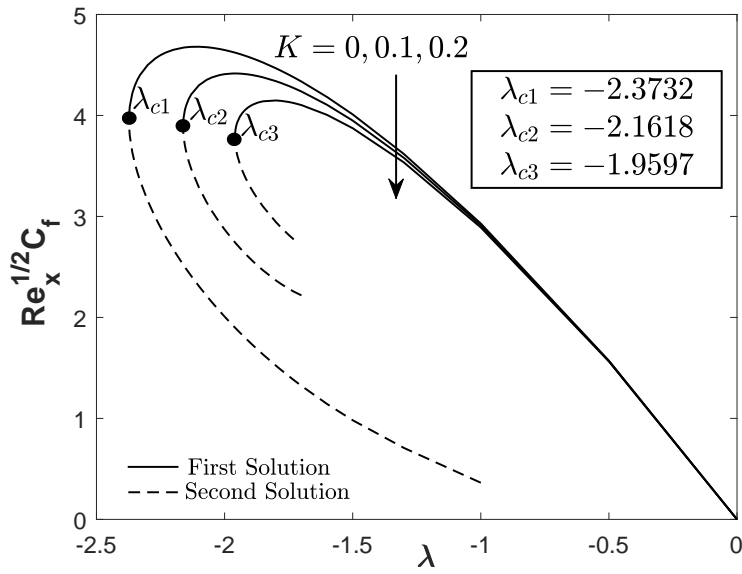


Figure 4. $Re_x^{1/2}C_f$ towards λ when $S = 3, \phi_1 = \phi_2 = 0.01$ and disparate values of the curvature parameter K .

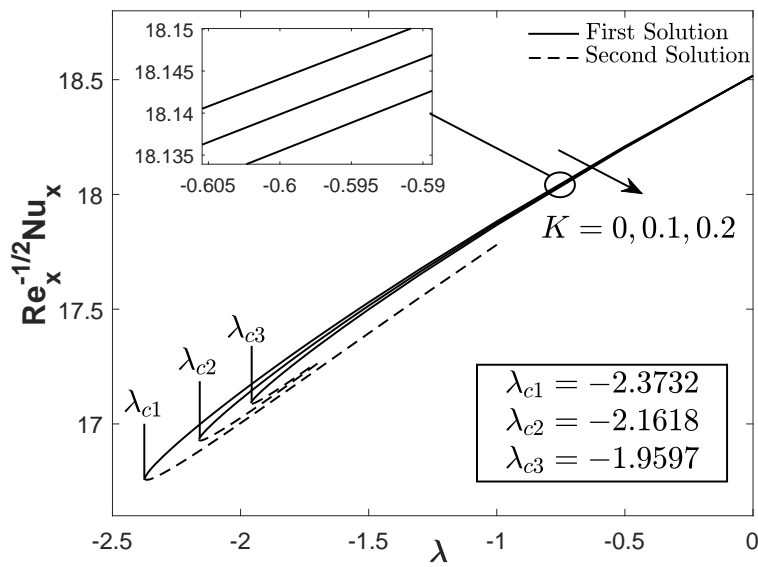


Figure 5. $Re_x^{-1/2}Nu_x$ towards λ when $S = 3, \phi_1 = \phi_2 = 0.01$ and disparate values of the curvature parameter K .

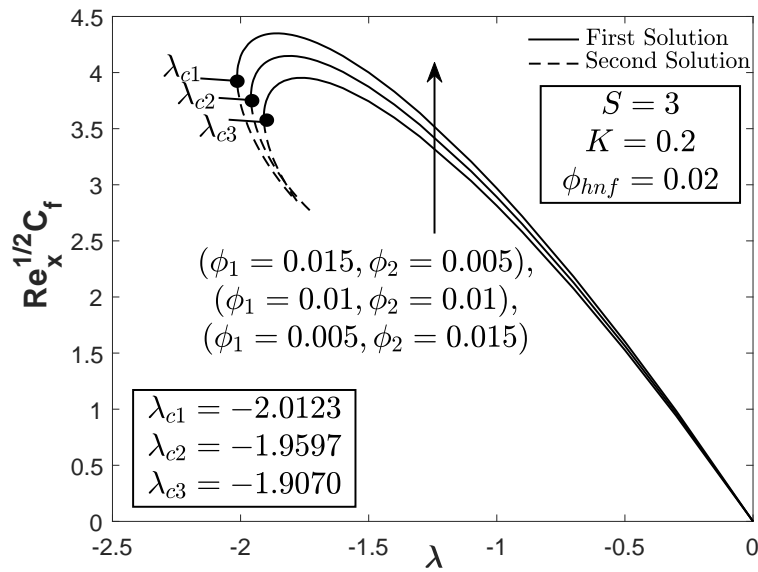


Figure 6. $Re_x^{1/2} C_f$ towards λ when $S = 3$, $K = 0.2$ and different volumetric concentrations of nanoparticles.

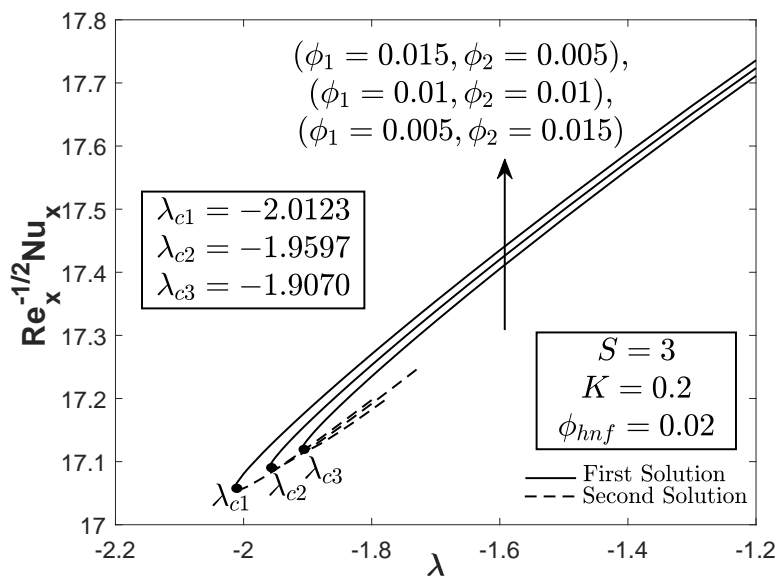


Figure 7. $Re_x^{-1/2} Nu_x$ towards λ when $S = 3$, $K = 0.2$ and different volumetric concentrations of nanoparticles.

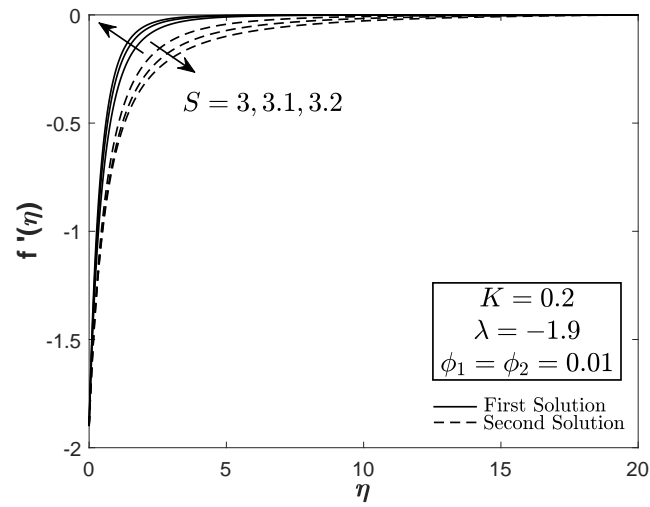


Figure 8. Impact of the suction parameter on the velocity profile.

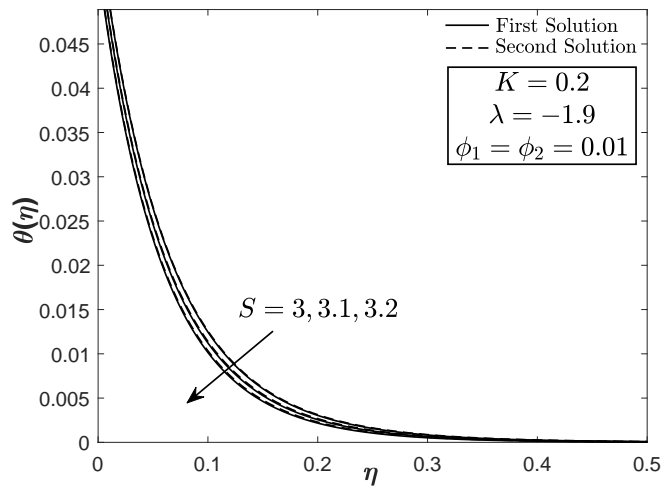


Figure 9. Impact of the suction parameter on the temperature profile.

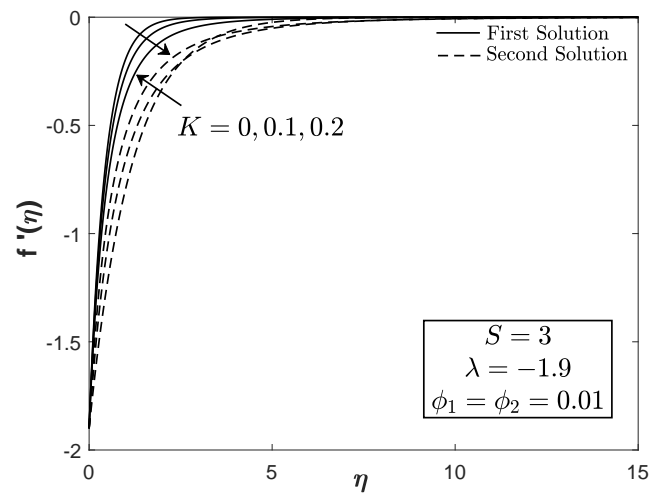


Figure 10. Impact of the curvature parameter on the velocity profile.

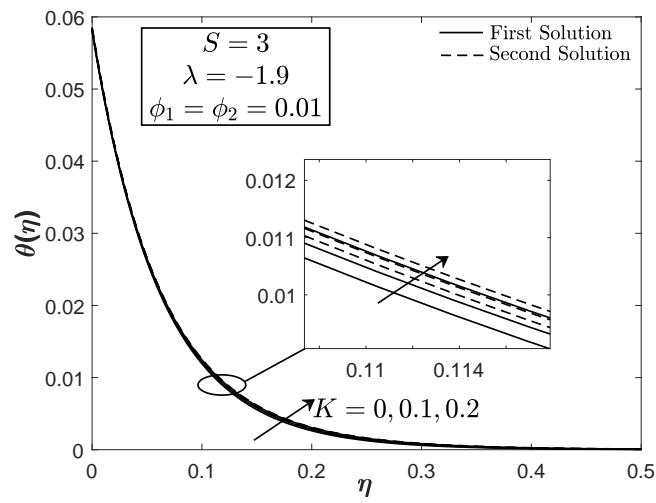


Figure 11. Impact of the curvature parameter on the temperature profile.

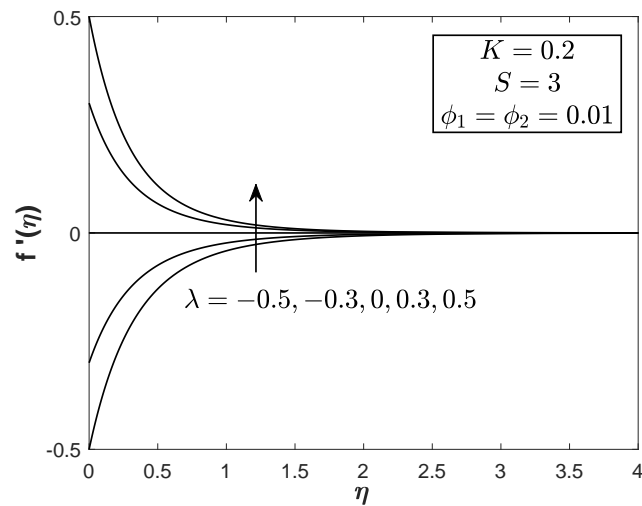


Figure 12. Impact of the stretching/shrinking parameter on the velocity profile.

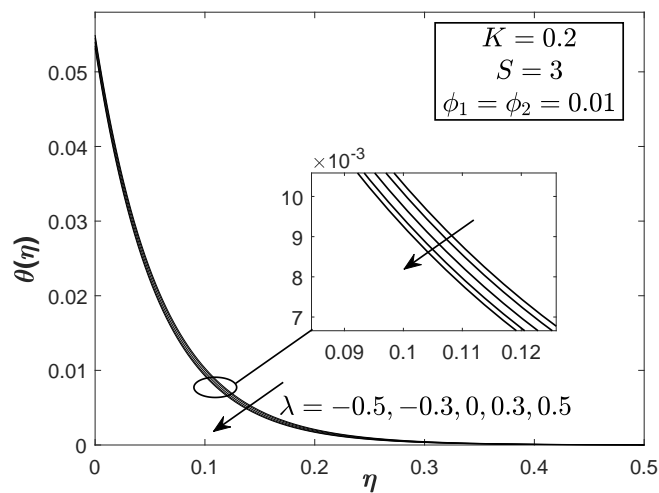


Figure 13. Impact of the stretching/shrinking parameter on the temperature profile.

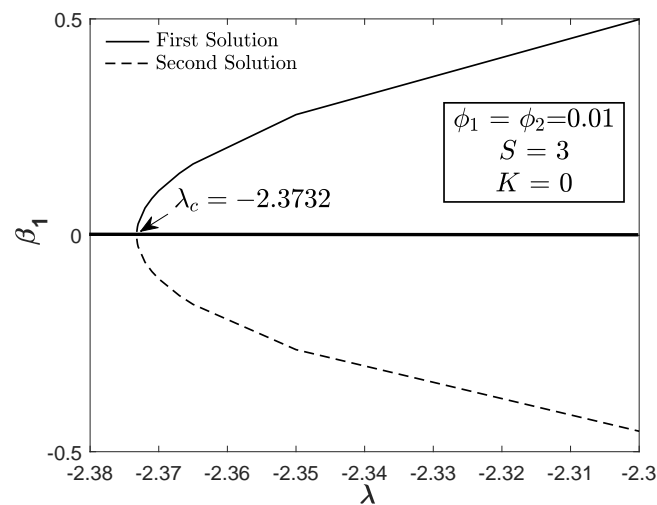


Figure 14. Smallest eigenvalue β_1 towards λ .

5. Conclusions

The present work scrutinized the laminar and two-dimensional Al_2O_3 -Cu/water nanofluid flow and heat transfer towards a permeable stretching/shrinking cylinder with prescribed surface heat flux. The respective differential equations can be reduced to a flat plate case when the curvature parameter $K = 0$, while $K > 0$ represents a circular cylinder surface. The conclusions are:

- For both shrinking cylinder and flat plate surfaces with the prescribed surface heat flux, the steady flow solutions are obtainable when the suction parameter is $S > 2.6$. No second solution was observed when considering the stretching surface.
- The separation of boundary layer can be decelerated by the extension of the critical value when $K = 0$. The flat plate surface also contributes to the maximum heat transfer rate.
- Among the three sets of hybrid Al_2O_3 -Cu nanoparticle concentrations such that $(\phi_1 = 0.5\%, \phi_2 = 1.5\%)$, $(\phi_1 = 1\%, \phi_2 = 1\%)$ and $(\phi_1 = 1.5\%, \phi_2 = 0.5\%)$, the hybrid nanofluids with concentration $(\phi_1 = 0.5\%, \phi_2 = 1.5\%)$ provided the greatest heat transfer rate and skin friction coefficient.
- The stability analysis mathematically supports the reliability of the first solution.
- The hybrid nanofluid flow due to the shrinking surfaces is a reverse (opposite) flow from the stretching surfaces. The velocity profile for the shrinking case ($\lambda < 0$) shows a negative value and contradicts the positive velocity profile for the stretching case ($\lambda > 0$).
- The hybrid nanofluid temperature for the stretching case is lower than the shrinking case.

6. Recommendations for Future Work

The present findings are limited to the combination of Al_2O_3 and Cu nanoparticles only with $\phi_{hmf} = 2\%$. For future work, it will be worth studying the significance of the cylinder in augmenting the heat transfer rate while delaying the separation of boundary layer flow by considering:

- Different hybrid nanofluids (other stable combinations based on the experimental work of hybrid nanofluids);
- Stagnation point flow (exclusion of the wall mass suction parameter);
- Other physical parameters, such as magnetic field, thermal radiation, viscous dissipation and Joule heating.

Author Contributions: N.S.K. and I.W., research design; N.S.K. and I.W., formulation and methodology; N.S.K., result analysis and validation; N.S.K., N.A.Z., K.H. and A.R.M.K., article preparation; I.W., N.A.Z. and K.H., review and editing. All authors have read and agreed to the published version of the manuscript.

Funding: This research was funded by Universiti Teknikal Malaysia Melaka through JURNAL/2019/FTKMP/Q00042.

Acknowledgments: The authors gratefully acknowledge Universiti Teknikal Malaysia Melaka for the financial support (JURNAL/2019/FTKMP/Q00042). The financial support was partially received from the Universiti Malaysia Pahang (Project Code: RDU182307).

Conflicts of Interest: There are no conflict of interest between the authors.

References

1. Zokri, S.M.; Arifin, N.S.; Mohamed, M.K.A.; Salleh, M.Z.; Kasim, A.R.M.; Mohammad, N.F. Influence of radiation and viscous dissipation on magnetohydrodynamic Jeffrey fluid over a stretching sheet with convective boundary conditions. *Malays. J. Fundam. Appl. Sci.* **2017**, *13*, 279–284. [\[CrossRef\]](#)
2. Khashi'ie, N.S.; Arifin, N.M.; Nazar, R.; Hafidzuddin, E.H.; Wahi, N.; Pop I. Mixed convective flow and heat transfer of a dual stratified micropolar fluid induced by a permeable stretching/shrinking sheet. *Entropy* **2019**, *21*, 1162. [\[CrossRef\]](#)
3. Kasim, A.R.M.; Arifin, N.S.; Zokri, S.M.; Salleh, M.Z. The investigation of a fluid-solid interaction mathematical model under combined convective jeffrey flow and radiation effect embedded newtonian heating as the thermal boundary condition over a vertical stretching sheet. *Defect Diffus. Forum* **2020**, *399*, 65–75. [\[CrossRef\]](#)
4. Khashi'ie, N.S.; Arifin, N.M.; Rashidi, M.M.; Hafidzuddin, E.H.; Wahi, N. Magnetohydrodynamics (MHD) stagnation point flow past a shrinking/stretching surface with double stratification effect in a porous medium. *J. Therm. Anal. Calorim.* **2020**, *139*, 3635–3648. [\[CrossRef\]](#)
5. Salleh, M.Z.; Mohamed, N.; Khairuddin, R.; Khashi'ie, N.S.; Nazar, R.; Pop, I. Free convection over a permeable horizontal flat plate embedded in a porous medium with radiation effects and mixed thermal boundary conditions. *J. Math. Stat.* **2012**, *8*, 122–128.
6. Choi, S.U.; Eastman, J.A. Enhancing thermal conductivity of fluids with nanoparticles. *ASME Fluids Eng. Div.* **1995**, *231*, 99–105.
7. Wang, Y.; Su, G.H. Experimental investigation on nanofluid flow boiling heat transfer in a vertical tube under different pressure conditions. *Exp. Therm. Fluid Sci.* **2016**, *77*, 116–123. [\[CrossRef\]](#)
8. Wang, Y.; Deng, K.H.; Liu, B.; Wu, J.M.; Su, G.H. A correlation of nanofluid flow boiling heat transfer based on the experimental results of AlN/H₂O and Al₂O₃/H₂O nanofluid. *Exp. Therm. Fluid Sci.* **2017**, *80*, 376–383. [\[CrossRef\]](#)
9. Ahmadi, M.; Willing, G. Heat transfer measurement in water based nanofluids. *Int. J. Heat Mass Transf.* **2018**, *118*, 40–47. [\[CrossRef\]](#)
10. Masuda, H.; Ebata, A.; Teramae, K. Alteration of thermal conductivity and viscosity of liquid by dispersing ultra-fine particles. *Netsu Bussei* **1993**, *4*, 227–233. [\[CrossRef\]](#)
11. Das, S.K.; Putra, N.; Thiesen, P.; Roetzel, W. Temperature dependence of thermal conductivity enhancement for nanofluids. *J. Heat Transf.* **2003**, *125*, 567–574. [\[CrossRef\]](#)
12. Pak, B.C.; Cho, Y.I. Hydrodynamic and heat transfer study of dispersed fluids with submicron metallic oxide particles. *Exp. Heat Transf. Int. J.* **1998**, *11*, 151–170. [\[CrossRef\]](#)
13. Kuznetsov, A.V.; Nield, D.A. Natural convective boundary-layer flow of a nanofluid past a vertical plate. *Int. J. Therm. Sci.* **2010**, *49*, 243–247. [\[CrossRef\]](#)
14. Mahat, R.; Rawi, N.A.; Kasim, A.R.M.; Shafie, S. Mixed convection flow of viscoelastic nanofluid past a horizontal circular cylinder with viscous dissipation. *Sains Malays.* **2018**, *47*, 1617–1623. [\[CrossRef\]](#)
15. Zokri, S.M.; Arifin, N.S.; Kasim, A.M.; Salleh, M.Z. Passive control of nanoparticles on MHD Jeffrey nanofluid past a convectively heated moving plate with thermal radiation. *Int. J. Automot. Mech. Eng.* **2018**, *15*, 5775–5792.
16. Waini, I.; Ishak, A.; Pop, I. Dufour and Soret effects on Al₂O₃-water nanofluid flow over a moving thin needle: Tiwari and Das model. *Int. J. Numer. Methods Heat Fluid Flow* **2020**. [\[CrossRef\]](#)
17. Waini, I.; Ishak, A.; Pop, I. Hybrid nanofluid flow past a permeable moving thin needle. *Mathematics* **2020**, *8*, 612. [\[CrossRef\]](#)
18. Waini, I.; Ishak, A.; Pop, I. Squeezed Hybrid Nanofluid Flow Over a Permeable Sensor Surface. *Mathematics* **2020**, *8*, 898. [\[CrossRef\]](#)

19. Khashi'ie, N.S.; Arifin, N.M.; Pop, I. Mixed Convective Stagnation Point Flow towards a Vertical Riga Plate in Hybrid Cu-Al₂O₃/Water Nanofluid. *Mathematics* **2020**, *8*, 912. [[CrossRef](#)]
20. Khashi'ie, N.S.; Arifin, N.M.; Pop, I.; Wahid, N.S. Flow and heat transfer of hybrid nanofluid over a permeable shrinking cylinder with Joule heating: A comparative analysis. *Alex. Eng. J.* **2020**, *59*, 1787–1798. [[CrossRef](#)]
21. Zainal, N.A.; Nazar, R.; Naganthran, K.; Pop, I. Unsteady Three-Dimensional MHD NonAxisymmetric Homann Stagnation Point Flow of a Hybrid Nanofluid with Stability Analysis. *Mathematics* **2020**, *8*, 784. [[CrossRef](#)]
22. Zainal, N.A.; Nazar, R.; Naganthran, K.; Pop, I. MHD flow and heat transfer of hybrid nanofluid over a permeable moving surface in the presence of thermal radiation. *Int. J. Numer Methods Heat Fluid Flow* **2020**. [[CrossRef](#)]
23. Zainal, N.A.; Nazar, R.; Naganthran, K.; Pop, I. MHD mixed convection stagnation point flow of a hybrid nanofluid past a vertical flat plate with convective boundary condition. *Chin. J. Phys.* **2020**, *66*, 630–644. [[CrossRef](#)]
24. Yen, T.H.; Soong, C.Y.; Tzeng, P.Y. Hybrid molecular dynamics-continuum simulation for nano/mesoscale channel flows. *Microfluid. Nanofluid.* **2007**, *3*, 665–675. [[CrossRef](#)]
25. Labib, M.N.; Nine, M.J.; Afrianto, H.; Chung, H.; Jeong, H. Numerical investigation on effect of base fluids and hybrid nanofluid in forced convective heat transfer. *Int. J. Therm. Sci.* **2013**, *71*, 163–171. [[CrossRef](#)]
26. Nasrin, R.; Alim, M.A. Finite element simulation of forced convection in a flat plate solar collector: influence of nanofluid with double nanoparticles. *J. Appl. Fluid Mech.* **2014**, *7*, 543–556.
27. Takabi, B.; Shokouhmand, H. Effects of Al₂O₃-Cu/water hybrid nanofluid on heat transfer and flow characteristics in turbulent regime. *Int. J. Mod. Phys. C* **2015**, *26*, 1550047. [[CrossRef](#)]
28. Devi, S.S.U.; Devi, S.A. Numerical investigation of three-dimensional hybrid Cu-Al₂O₃/water nanofluid flow over a stretching sheet with effecting Lorentz force subject to Newtonian heating. *Can. J. Phys.* **2016**, *94*, 490–496. [[CrossRef](#)]
29. Devi, S.S.U.; Devi, S.A. Heat transfer enhancement of Cu-Al₂O₃/water hybrid nanofluid flow over a stretching sheet. *J. Niger. Math. Soc.* **2017**, *36*, 419–433.
30. Yousefi, M.; Dinarvand, S.; Yazdi, M.E.; Pop, I. Stagnation-point flow of an aqueous titania-copper hybrid nanofluid toward a wavy cylinder. *Int. J. Numer. Methods Heat Fluid Flow* **2018**, *28*, 1716–1735. [[CrossRef](#)]
31. Hayat, T.; Nadeem, S.; Khan, A.U. Rotating flow of Ag-CuO/H₂O hybrid nanofluid with radiation and partial slip boundary effects. *Eur. Phys. J. E* **2018**, *41*, 75. [[CrossRef](#)] [[PubMed](#)]
32. Ghadikolaei, S.S.; Yassari, M.; Sadeghi, H.; Hosseinzadeh, K.; Ganji, D.D. Investigation on thermophysical properties of TiO₂-Cu/H₂O hybrid nanofluid transport dependent on shape factor in MHD stagnation point flow. *Powder Technol.* **2017**, *322*, 428–438. [[CrossRef](#)]
33. Tayebi, T.; Chamkha, A.J. Buoyancy-driven heat transfer enhancement in a sinusoidally heated enclosure utilizing hybrid nanofluid. *Comp. Therm. Sci. Int. J.* **2017**, *9*, 405–421. [[CrossRef](#)]
34. Ashorynejad, H.R.; Shahriari, A. MHD natural convection of hybrid nanofluid in an open wavy cavity. *Results Phys.* **2018**, *9*, 440–455. [[CrossRef](#)]
35. Kasim, A.R.M.; Arifin, N.S.; Ariffin, N.A.N.; Salleh, M.Z.; Anwar, M.I. Mathematical model of simultaneous flow between casson fluid and dust particle over a vertical stretching sheet. *Int. J. Integr. Eng.* **2020**, *12*, 253–260.
36. Lund, L.A.; Omar, Z.; Khan, U.; Khan, I.; Baleanu, D.; Nisar, K.S. Stability analysis and dual solutions of micropolar nanofluid over the inclined stretching/shrinking surface with convective boundary condition. *Symmetry* **2020**, *12*, 74. [[CrossRef](#)]
37. Waini, I.; Ishak, A.; Pop, I. Hybrid nanofluid flow induced by an exponentially shrinking sheet. *Chin. J. Phys.* **2019**, in press. [[CrossRef](#)]
38. Anuar, N.S.; Bachok, N.; Arifin, N.M.; Rosali, H. Effect of Suction/Injection on Stagnation Point Flow of Hybrid Nanofluid over an Exponentially Shrinking Sheet with Stability Analysis. *CDF Lett.* **2019**, *11*, 21–33.
39. Wang, C.Y. Fluid flow due to a stretching cylinder. *Phys. Fluids* **1988**, *31*, 466–468. [[CrossRef](#)]
40. Mukhopadhyay, S. Mixed convection boundary layer flow along a stretching cylinder in porous medium. *J. Pet. Sci. Eng.* **2012**, *96*, 73–78. [[CrossRef](#)]
41. Vajravelu, K.; Prasad, K.V.; Santhi, S.R. Axisymmetric magneto-hydrodynamic (MHD) flow and heat transfer at a non-isothermal stretching cylinder. *Appl. Math. Comput.* **2012**, *219*, 3993–4005. [[CrossRef](#)]

42. Butt, A.S.; Ali, A. Entropy analysis of magnetohydrodynamic flow and heat transfer due to a stretching cylinder. *J. Taiwan Inst. Chem. Eng.* **2014**, *45*, 780–786. [[CrossRef](#)]
43. Abbas, Z.; Rasool, S.; Rashidi, M.M. Heat transfer analysis due to an unsteady stretching/shrinking cylinder with partial slip condition and suction. *Ain Shams Eng. J.* **2015**, *6*, 939–945. [[CrossRef](#)]
44. Malik, M.Y.; Salahuddin, T.; Hussain, A.; Bilal, S.; Awais, M. Homogeneous-heterogeneous reactions in Williamson fluid model over a stretching cylinder by using Keller box method. *AIP Adv.* **2015**, *5*, 107227. [[CrossRef](#)]
45. Shafiq, A.; Khan, I.; Rasool, G.; Seikh, A.H.; Sherif, E.S.M. Significance of double stratification in stagnation point flow of third-grade fluid towards a radiative stretching cylinder. *Mathematics* **2019**, *7*, 1103. [[CrossRef](#)]
46. Ganesan, P.; Loganathan, P. Magnetic field effect on a moving vertical cylinder with constant heat flux. *Heat Mass Transf.* **2003**, *39*, 381–386. [[CrossRef](#)]
47. Ferdows, M.; Reddy, M.G.; Alzahrani, F.; Sun, S. Heat and Mass Transfer in a Viscous Nanofluid Containing a Gyrotactic Micro-Organism Over a Stretching Cylinder. *Symmetry* **2019**, *11*, 1131. [[CrossRef](#)]
48. Ullah, I.; Alkanhal, T.A.; Shafie, S.; Nisar, K.S.; Khan, I.; Makinde, O.D. MHD Slip Flow of Casson Fluid along a Nonlinear Permeable Stretching Cylinder Saturated in a Porous Medium with Chemical Reaction, Viscous Dissipation, and Heat Generation/Absorption. *Symmetry* **2019**, *11*, 531. [[CrossRef](#)]
49. Suleman, M.; Ramzan, M.; Ahmad, S.; Lu, D.; Muhammad, T.; Chung, J.D. A Numerical Simulation of Silver–Water Nanofluid Flow with Impacts of Newtonian Heating and Homogeneous–Heterogeneous Reactions Past a Nonlinear Stretched Cylinder. *Symmetry* **2019**, *11*, 295. [[CrossRef](#)]
50. Muthamilselvan, M.; Prakash, D. Unsteady hydromagnetic slip flow and heat transfer of nanofluid over a moving surface with prescribed heat and mass fluxes. *Proc. Inst. Mech. Eng. Part J. Mech. Eng. Sci.* **2015**, *229*, 703–715. [[CrossRef](#)]
51. Jalilpour, B.; Jafarmadar, S.; Ganji, D.D.; Shotorban, A.B.; Taghavifar, H. Heat generation/absorption on MHD stagnation flow of nanofluid towards a porous stretching sheet with prescribed surface heat flux. *J. Mol. Liq.* **2014**, *195*, 194–204. [[CrossRef](#)]
52. Waini, I.; Ishak, A.; Pop, I. On the stability of the flow and heat transfer over a moving thin needle with prescribed surface heat flux. *Chin. J. Phys.* **2019**, *60*, 651–658. [[CrossRef](#)]
53. Kasim, A.R.M.; Mohammad, N.F.; Shafie, S.; Pop, I. Constant heat flux solution for mixed convection boundary layer viscoelastic fluid. *Heat Mass Transf.* **2013**, *49*, 163–171. [[CrossRef](#)]
54. Waini, I.; Ishak, A.; Pop, I. Hybrid nanofluid flow and heat transfer past a vertical thin needle with prescribed surface heat flux. *Int. J. Numer. Methods Heat Fluid Flow* **2019**, *29*, 4875–4894. [[CrossRef](#)]
55. Kasim, A.R.M.; Mohammad, N.F.; Shafie, S. Effect of heat generation on free convection boundary layer flow of a viscoelastic fluid past a horizontal circular cylinder with constant surface heat flux. *AIP Conf. Proc.* **2012**, *1450*, 286–292.
56. Tiwari, R.K.; Das, M.K. Heat transfer augmentation in a two-sided lid-driven differentially heated square cavity utilizing nanofluids. *Int. J. Heat Mass Transf.* **2007**, *50*, 2002–2018. [[CrossRef](#)]
57. Qasim, M.; Khan, Z.H.; Khan, W.A.; Shah, I.A. MHD boundary layer slip flow and heat transfer of ferrofluid along a stretching cylinder with prescribed heat flux. *PLoS ONE* **2014**, *9*, e83930. [[CrossRef](#)]
58. Takabi, B.; Salehi, S. Augmentation of the heat transfer performance of a sinusoidal corrugated enclosure by employing hybrid nanofluid. *Adv. Mech. Eng.* **2014**, *6*, 147059. [[CrossRef](#)]
59. Oztop, H.F.; Abu-Nada, E. Numerical study of natural convection in partially heated rectangular enclosures filled with nanofluids. *Int. J. Heat Fluid Flow* **2008**, *29*, 1326–1336. [[CrossRef](#)]
60. Sankar Giri, S.; Das, K.; Kundu, P.K. Homogeneous–heterogeneous reaction mechanism on MHD carbon nanotube flow over a stretching cylinder with prescribed heat flux using differential transform method. *J. Comput. Des. Eng.* **2020**, *7*, 337–351. [[CrossRef](#)]
61. Merkin, J.H. On dual solutions occurring in mixed convection in a porous medium. *J. Eng. Math.* **1986**, *20*, 171–179. [[CrossRef](#)]
62. Weidman, P.D.; Kubitschek, D.G.; Davis, A.M.J. The effect of transpiration on self-similar boundary layer flow over moving surfaces. *Int. J. Eng. Sci.* **2006**, *44*, 730–737. [[CrossRef](#)]
63. Harris, S.D.; Ingham, D.B.; Pop, I. Mixed convection boundary-layer flow near the stagnation point on a vertical surface in a porous medium: Brinkman model with slip. *Transp. Porous Media* **2009**, *77*, 267–285. [[CrossRef](#)]

64. Suresh, S.; Venkataraj, K.P.; Selvakumar, P.; Chandrasekar, M. Synthesis of Al₂O₃-Cu/water hybrid nanofluids using two step method and its thermo physical properties. *Colloids Surf. Physicochem. Eng. Asp.* **2011**, *388*, 41–48. [[CrossRef](#)]
65. Khashi'ie, N.S.; Arifin, N.M.; Pop, I.; Nazar, R.; Hafidzuddin, E.H.; Wahi, N. Flow and heat transfer past a permeable power-law deformable plate with orthogonal shear in a hybrid nanofluid. *Alex. Eng. J.* **2020**, *59*, 1869–1879. [[CrossRef](#)]
66. Bachok, N.; Ishak, A. Flow and heat transfer over a stretching cylinder with prescribed surface heat flux. *Malays. J. Math. Sci.* **2010**, *4*, 159–169.



© 2020 by the authors. Licensee MDPI, Basel, Switzerland. This article is an open access article distributed under the terms and conditions of the Creative Commons Attribution (CC BY) license (<http://creativecommons.org/licenses/by/4.0/>).